

Fast-frequency-hopping modulation and detection demonstration

M. R. Fetterman, J. C. Davis, H.-S. Tan, W. Yang, D. Goswami, J.-K. Rhee, and W. S. Warren

Princeton University Center for Ultrafast Laser Applications, Princeton University, Princeton, New Jersey 08544

Received August 24, 2000; revised manuscript received January 22, 2001

We demonstrate fast-frequency-hopping modulation that exploits the unique features of acousto-optic-modulator based laser pulse shaping and the spectrally and temporally resolved upconversion technique (STRUT) pulse-characterization method. These pulses have been specifically designed so that they can be characterized by the STRUT, without any processing of the STRUT data set. We present examples of complex fast-frequency-hopping laser pulses that have been generated and characterized by our pulse-shaping system and STRUT. We discuss the theoretical limitations on the data rate that can be obtained with such a technique. © 2001 Optical Society of America

OCIS codes: 320.5540, 060.4510.

1. INTRODUCTION

Ultrafast pulse-shaping systems have made it possible to shape pulses that are of the order of ten to hundreds of femtoseconds long in the spatio-temporal domain.¹⁻³ Ultrafast detection systems allow us to detect the amplitude and the phase of the shaped pulse.⁴⁻⁸

These shaped pulses can be used in various communications architectures. The three most common of these are wavelength-division multiplexing, time-division multiplexing, and code-division multiple access (CDMA). The choice of an architecture depends on the system requirements. In wavelength-division-multiplexing systems the spectral bandwidth is divided into wavelength channels. This spectra modulation increases the pulse length. Time-division-multiplexing systems, on the other hand, transmit pulses stacked in the time domain.

CDMA is perhaps the most versatile architecture, because it is a mix between time- and wavelength-division multiplexing. The CDMA system coding is described as a set of semi-orthogonal codes⁹:

$$c_k(t) = \sum d_{k,j} p_j(t - jT_c). \quad (1)$$

In this equation the user is denoted by k , and $d(k, j)$ is the j th value of the k th user's code. The variable $p_j(t)$ is the chip-signaling waveform. Fast-frequency hopping (FFH) CDMA⁹ is a variation of CDMA, in which each user receives a code within the spatio-temporal matrix. Assume that the matrix in Fig. 1, with q frequencies and N time slots, represents the pulse. Then any given pulse can be described by listing the appropriate set of numbers as described in Fig. 1. Because of the details of the detection system, the gray squares do not contain data, which is explained below.

In this paper we show the generation of FFH pulses, using the acousto-optic-modulator (AOM) pulse-shaping system. We show their detection using the STRUT⁴⁻⁷ detection system. The STRUT may be the most intuitive way to investigate both the time and frequency features of

these complex pulses, as the STRUT spectrogram requires no additional processing to do so. Using our current setup, we need to measure many spectra to acquire a pulse. In principle, however, the STRUT data acquisition can be done in a single shot. Since in this study we do not create or detect orthogonal pulses, we do not present the study in terms of CDMA communications. The pulse generation and detection that we show here could be used in a variety of different communications systems, including CDMA. We therefore refer to our pulses as FFH pulses.

2. ACOUSTO-OPTIC-MODULATOR PULSE SHAPING

The system layout for these experiments is shown schematically in Fig. 2 (lower), with the AOM pulse shaper inserted into a commercially available femtosecond Ti:sapphire oscillator and regenerative amplifier system. The oscillator (Mira, Coherent)¹⁰ is pumped with 8 W at 514 nm from a cw argon-ion laser (Innova 400, Coherent)¹⁰ to produce 110-fs pulses at a center wavelength of 795 nm. A typical spectral bandwidth of 10 nm is measured at the FWHM (full width at half-maximum). Each oscillator pulse has energy of approximately 13 nJ at a repetition rate of 76 MHz.

The oscillator output pulses are then injected into the Ti:sapphire regenerative amplifier (Clark/MXR¹¹) after having passed through the AOM pulse shaper to produce shaped and amplified pulses with 200 mJ of energy per pulse. We note that such an amplified pulse-shaping system is convenient but not necessary; the STRUT is capable of detecting the unamplified pulses as well. The amplifier uses the chirped pulse amplification technique and is pumped with a Q-switched frequency-doubled Nd:YAG at a repetition rate that was set to 1 kHz but can be set up to 50 kHz. By the chirped pulse amplification scheme, oscillator pulses (without shaping) are stretched to 150 ps, amplified, and compressed to 150 fs with 200 mJ of energy per pulse. The bandwidth is reduced to 8

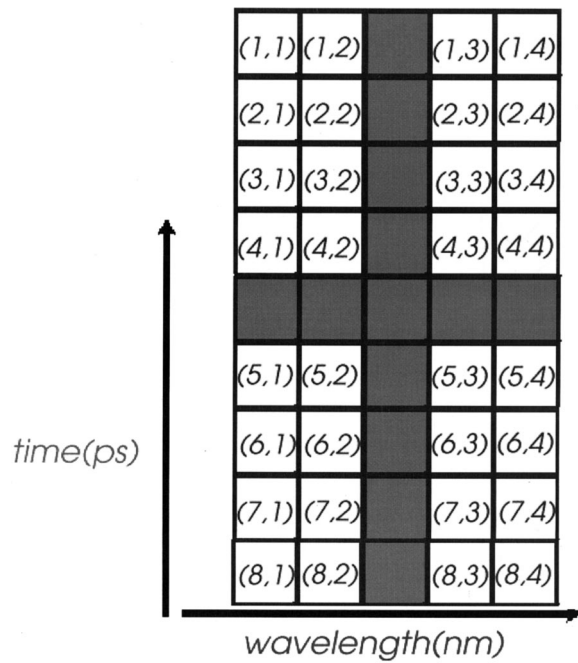


Fig. 1. Schematic drawing of the Wigner pulse. The numbers refer to matrix elements indexed by the temporal and the wavelength domains. As described in the text, because of the details of the detection system, the gray boxes cannot contain data.

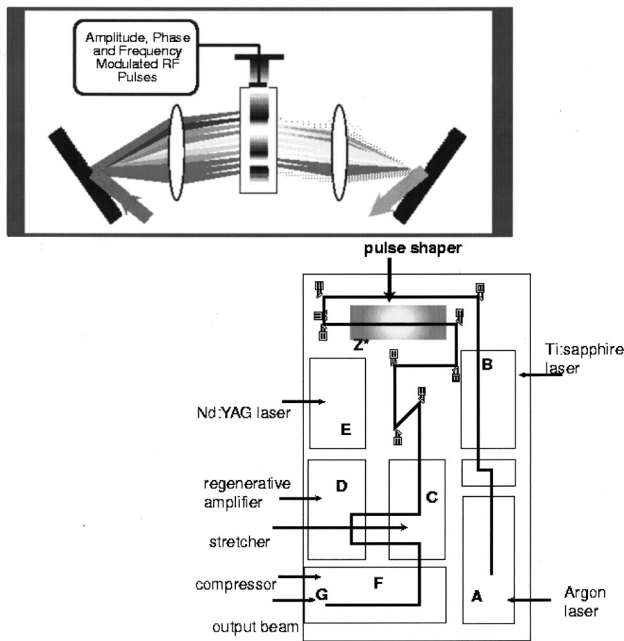


Fig. 2. System layout.

nm owing to gain-bandwidth narrowing. It is important to stretch the pulses adequately; otherwise, nonlinear effects will distort the shaped pulse in the regenerative amplifier.

The AOM pulse-shaping technology has been described in detail in previous research⁴⁻⁹ and consists of a zero-dispersion line and an AOM (Brimrose),¹² as shown schematically in Fig. 2 (upper). The broad spectrum of a femtosecond pulse is dispersed spatially by 1800-lines/mm gratings. It is then collimated with a 30-cm lens to form

a linear spectral image at the AOM crystal (the center of the 4-f system). Shaped RF (radio-frequency) pulses create the desired modulation pattern on the AOM. The shaped RF pulses⁹ are generated with an arbitrary function generator (LeCroy)¹³ with a resolution of 400 MHz. In this particular system a tellurium-dioxide (TeO_2) crystal is used in the AOM. The acoustic velocity of 4.2 mm/ms in TeO_2 is far slower than the speed of light, and consequently, with respect to the light pulse, the acoustic wave may be considered stationary. Thus the acoustic wave acts as a transmission diffraction grating.⁹ The AOM has a 40 mm \times 2.3 mm clear aperture size. The full width at half-maximum on the spectrum is approximately 30 nm on the AOM. The pulse shaper is inserted into the system as shown in Fig. 2 (lower), before the regenerative amplifier.

3. SPECTRALLY AND TEMPORALLY RESOLVED UPCONVERSION TECHNIQUE DETECTION

The STRUT has been discussed in previous research,⁴ so we only briefly summarize the relevant equations here. The input laser beam is split into two parts with a beam splitter: the test beam, E_t , and the reference beam, E_r . The test beam is delayed by a time τ , and the reference beam is spectrally filtered, as described below.

The reference beam is spread spectrally (and spatially) with a diffraction grating and filtered by a rectangular slit having the filter function $G(\omega)$. For the case of complex pulse shaping it is necessary to allow the spectral region defined by $G(\omega)$ to remain unmodulated. It is for this reason that the central regions of Fig. 1 contain no data and are shaded gray, signifying the unmodulated reference pulse. The electric fields of the reference and test beams are given by

$$E_r = G(\omega)A(\omega)\exp[i\phi(\omega)],$$

$$E_t = A(\omega)\exp[i\phi(\omega)].$$
(2)

Here, ω is the detuning from the central frequency, $A(\omega)$ is the envelope function, and $\phi(\omega)$ is the spectral phase. The reference pulse proceeds to travel around one arm of an interferometer while the test pulse travels around the other arm, the distance of which is varied systematically (thereby delaying the test pulse with respect to the reference pulse). The two pulses are then recombined in a second-harmonic crystal. Finally, the sum frequency is collected and directed into a spectrometer. The upconverted signal field at the second-harmonic crystal is denoted by $E_{\text{up}}(\tau, \omega)$:

$$E_{\text{up}}(\tau, \omega) \propto \int d\omega' E_r(\omega') \exp(i\omega'\tau) E_t(\omega - \omega').$$
(3)

In this equation, τ is the delay of the test pulse with respect to the reference pulse.

In general, it is necessary to analyze the STRUT data to recover the pulse characteristics (i.e., its phase, spectrum, and temporal profile). However, because of the way that we designed our input signal, it was not necessary to perform any analysis on the STRUT data. All of the STRUT data that we show in this paper are unproc-

essed, which means that all of the necessary information is present in the STRUT spectrogram itself. Although in this case the STRUT detection system requires taking multiple spectra, it is possible to construct a single-shot STRUT with a higher-efficiency second-harmonic generation crystal.

4. RESULTS AND ANALYSIS

In Fig. 1 we divided the matrix $W(a, b) = W(1...4, 1...8)$ into 32 regions, where a indexes wavelengths 1–4 and b indexes times 1–8. The central region of the pulse is not labeled for the reason described above. Each region has an equal width $\Delta\omega$ in the spectral domain. The temporal width of each region is given by Δt , such that each individual region is transform limited. Each point $W(a, b)$ corresponds to a bit in a communications channel that may be either on or off.

We were able to encode four features in the frequency domain and eight features in the time domain of our 100-fs laser pulses. Using the AOM pulse-shaping technique, as well as the STRUT detection system, we could individually control the features in the time–frequency matrix $W(a, b)$.

The elements in $W(a, b)$ correspond to modulated laser pulses in the following way: A delay in time between laser pulses in a pulse train corresponds to a linear phase shift in the frequencies of these pulses.¹⁴ Consider the matrix element 1 of Fig. 1. If ω_1 and ω_2 denote the points in frequency space that bound matrix element 1, then the electric field that corresponds to this laser pulse is given by

$$E(\omega) = A \exp(i\alpha\omega), \quad \omega_1 < \omega < \omega_2. \quad (4)$$

In Eq. (4) the constant α is equal to the timing offset of matrix element 1 from the central matrix element. The constant A represents the envelope amplitude of the laser

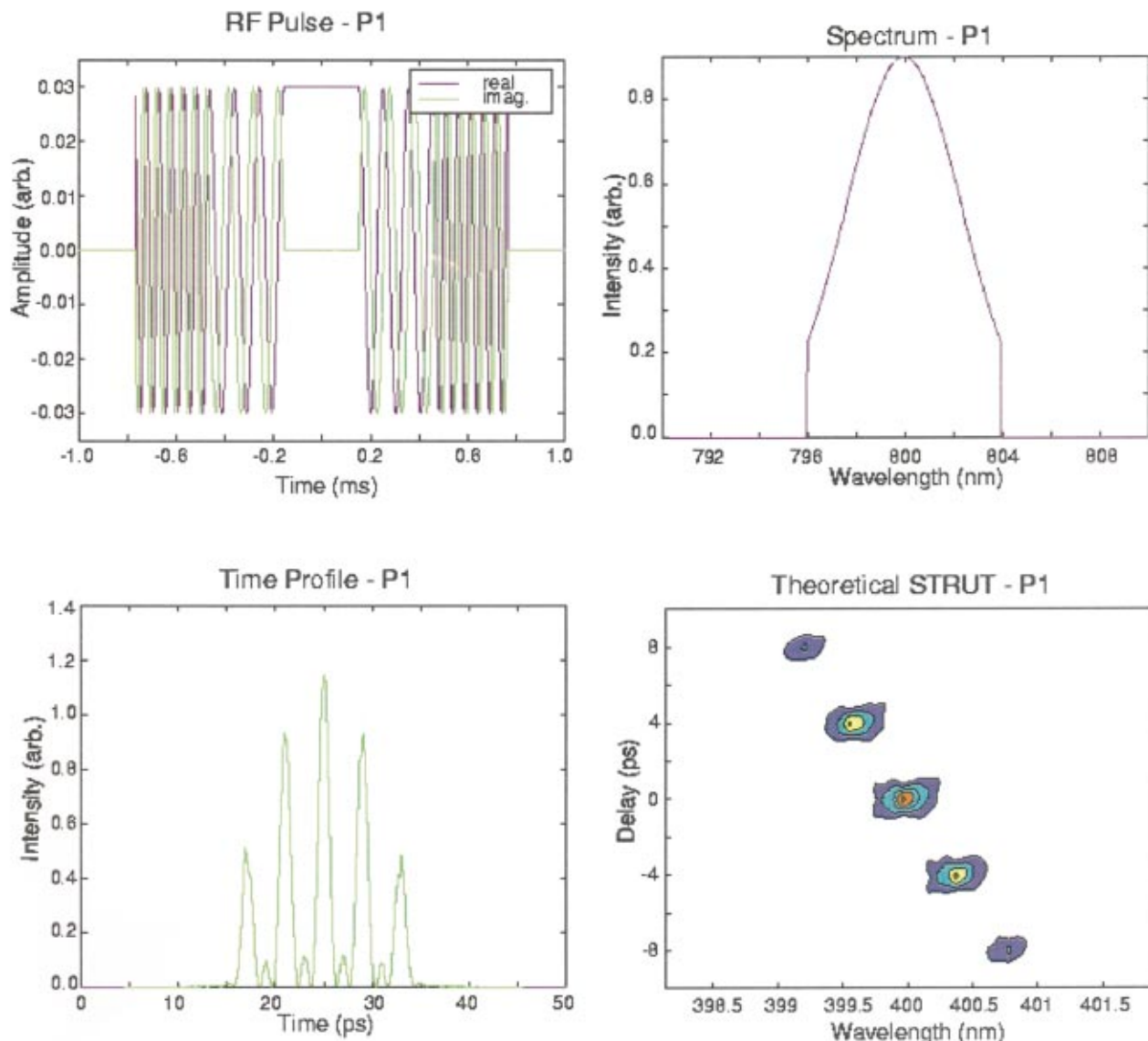


Fig. 3. Theoretical results for pulse P1: (upper left) RF waveform used to generate the pulse; (upper right) spectrum of P1; (lower left) temporal profile of P1; (lower right) STRUT for P1.

pulse and may be predistorted.¹ Since the electric fields corresponding to different matrix elements can be summed linearly, the modulated field is simply $\sum_i E_i(\omega)$.

We studied two FFH-modulated pulses both theoretically and experimentally. The matrix elements of these pulses (denoted P_1 and P_2) are given below. The numbers indicated for P_1 and P_2 reference those elements of the time-wavelength matrix shown in Fig. 1 that are on (all matrix elements not included in P_1 and P_2 should be considered off). Here, the element X (the reference pulse for the STRUT) indicates the wavelength component at the center frequency. This X element is the reference pulse for the STRUT. This explains why we cannot transmit data in the vertical gray squares in Fig. 1. Because the width of the pulse in the central square exceeds the width of one square, we are prevented from using the central row in Fig. 1 for data transmission.

$$P_1 : W = 1, 10, X, 23, 32, \quad (5)$$

$$P_2 : W = 1, 4, 6, 7, 9, 12, 14, 15, X, 18, 19, 21, \\ 24, 25, 28, 30, 31. \quad (6)$$

In Fig. 3, a theoretical STRUT of P_1 is illustrated (lower right) in addition to the RF waveform used to generate the laser pulse (upper left), the P_1 spectrum (upper right), and its temporal profile (lower left).

The experimental STRUT trace that corresponds to the pulse P_1 is illustrated in Fig. 4. Note that this STRUT trace is the raw data without processing. We have added grid lines to this figure to clarify analysis of the features contained therein. Clearly, all five features of P_1 are recovered in the spectrogram. The signal-to-noise ratio for this trace is approximately 10 dB in the worst-case situation of a matrix segment "on" next to a matrix segment "off." The axes of Fig. 4 show that each matrix element has a width of approximately 0.4 nm by 1.5 ps, which corresponds to an area of 1.12 (bits/s)/Hz. This value is remarkably close to the theoretical limit derived below.

Figure 5 shows the theoretical STRUT trace for the pulse P_2 , and in Fig. 6 we present the experimental STRUT trace corresponding to pulse P_2 . There are 16 features (in addition to the reference pulse in the center) that can be recovered from this trace. The signal-to-noise ratio for this case is 3 dB. The area per bit for Fig.

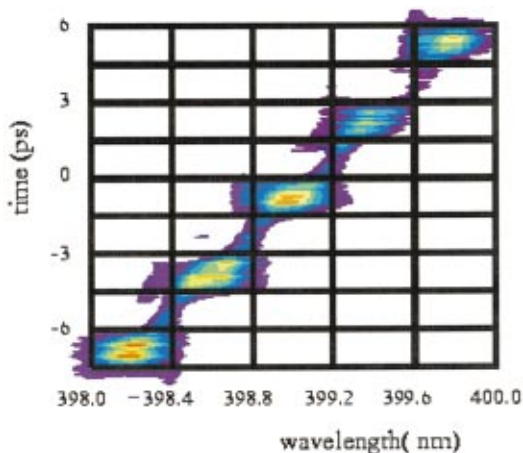


Fig. 4. Experimental STRUT result for the pulse P_1 .

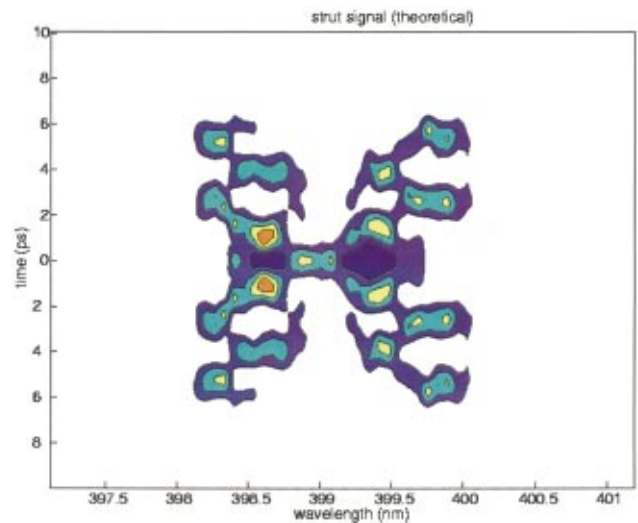


Fig. 5. Theoretical STRUT calculated for pulse P_2 .

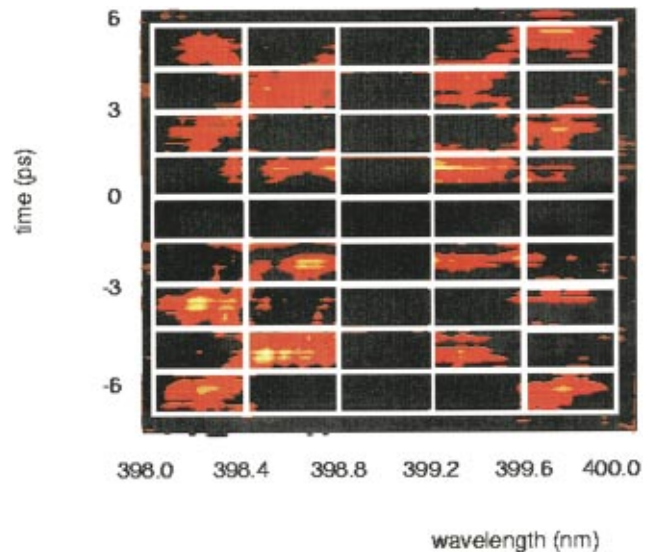


Fig. 6. Experimental STRUT result for the pulse P_2 .

5 is the same as for Fig. 4. It appears that, for a complex pulse such as P_2 , which contains a high density of features (information), the signal-to-noise ratio degrades. It should be noted that with the STRUT detection method for this modulation scheme the relative phase between the delayed pulses cannot be resolved. This would be problematic in cases such as wave-packet interferometry experiments,^{15,16} in which knowledge of the phase relation between the pulses is crucial.

Owing to the STRUT's inherent upconversion element, its incorporation into a FFH communications protocol as a (very convenient) detection device lowers the upper limit of spectral efficiency. The spectral efficiency for this modulation scheme (i.e., with a waveform such as P_2 and the STRUT detection system) can be calculated in the following way: If square pulses are assumed for the reference and the probe pulses, and the spectral widths of these pulses are β and α , respectively, the probe pulse, centered at ω_p^0 , can be written

$$E_p(\omega) \propto \begin{cases} 1 & \omega_p^0 - \frac{\alpha}{2} \leq \omega \leq \omega_p^0 + \frac{\alpha}{2}, \\ 0 & \text{rest of the universe} \end{cases} \quad (7)$$

and the reference pulse, centered at ω_r^0 , is similarly

$$E_r(\omega) \propto \begin{cases} 1 & \omega_r^0 - \frac{\beta}{2} \leq \omega \leq \omega_r^0 + \frac{\beta}{2}, \\ 0 & \text{rest of the universe} \end{cases} \quad (8)$$

The intensity of the STRUT trace for these pulses is then

$$I(\Omega, \tau) = \left| \int_{-\infty}^{\infty} d\omega_r E_r(\omega_r) E_p(\omega_p = \Omega - \omega_r) \times \exp[i(\Omega - \omega_r)\tau] \right|^2, \quad (9)$$

where Ω is the frequency of the upconverted signal and τ is the STRUT time coordinate. Evaluating the integral in Eq. (9) leads to an expression for $I(\Omega', \tau)$, where $\Omega' = (\omega_r^0 - \omega_p^0)$;

$$I(\Omega', \tau) \propto \begin{cases} \frac{\sin^2\left[\left(\Omega' - \frac{1}{2}(\alpha + \beta)\right)\frac{\tau}{2}\right]}{\tau^2} & \frac{1}{2}(\alpha + \beta) \geq \Omega' > \frac{1}{2}(\alpha - \beta) \\ \frac{\sin^2\left(\frac{\beta\tau}{2}\right)}{\tau^2} & \frac{1}{2}(\alpha - \beta) \geq \Omega' \geq -\frac{1}{2}(\alpha - \beta) \\ \frac{\sin^2\left[\left(\Omega' + \frac{1}{2}(\alpha + \beta)\right)\frac{\tau}{2}\right]}{\tau^2} & -\frac{1}{2}(\alpha - \beta) > \Omega' \geq -\frac{1}{2}(\alpha + \beta) \end{cases} \quad (10)$$

The FWHM of the probe pulse in the time domain is minimized when α is set equal to β . In this case,

$$I(\Omega', \tau) \propto \frac{\sin^2\left[\left(\alpha - |\Omega'|\right)\frac{\tau}{2}\right]}{\tau^2}. \quad (11)$$

From this expression the FWHM is found to be equal to $5.56/\alpha$, where α is in radians. Thus the upper-limit spectral efficiency, which we refer to as η , for the AOM-STRUT modulation method is 1.13 (bits/s)/Hz. If Gaussian pulses replace the square pulses in the calculations above, η remains nearly the same at 1.133 (bits/s)/Hz. Because we were only able to use 32 of 45 matrix boxes for encoding information, the spectral efficiency of our experimental system (if FFH pulses were sent and detected consecutively, with no time interval between pulses) was

$\eta = 0.92$ (bits/s)/Hz. Even so, this spectral efficiency corresponds to a data-transmission rate of 4 Tbits/s.

5. CONCLUSION

In conclusion, we have discussed the modulation and the detection of FFH pulses, showing laser pulses that are shaped and detected in both the frequency and the time domains. The STRUT characterization allows us to study these pulses without processing the STRUT data. We also study the fundamental data-transmission limits for such pulses. We thank the reviewers for their helpful comments.

REFERENCES

1. M. R. Fetterman, D. Goswami, D. Keusters, W. Yang, J.-K. Rhee, and W. S. Warren, "Ultrafast pulse shaping: characterization and amplification," *Opt. Express* **310**, 366 (1998).
2. H. P. Sardesai and A. M. Weiner, "Nonlinear fiber-optic receiver for ultrashort pulse code division multiple access communications," *Electron. Lett.* **33**, 610–611 (1997).
3. M. Haner and W. Warren, "Synthesis of crafted optical pulses by time domain modulation in a fiber grating compressor," *Appl. Phys. Lett.* **52**, 1458 (1988).
4. J.-K. Rhee, T. S. Sosnowski, A. C. Tien, and T. B. Norris, "Real-time dispersion analyzer of femtosecond laser pulses with use of a spectrally and temporally resolved upconversion technique," *J. Opt. Soc. Am. B* **13**, 1780–1785 (1996).
5. J. L. A. Chilla and O. E. Martinez, "Direct determination of the amplitude and phase of femtosecond light pulses," *Opt. Lett.* **16**, 39–41 (1991).
6. D. T. Reid, "Algorithm for complete and rapid retrieval of ultrashort pulse amplitude and phase from a sonogram," *IEEE J. Quantum Electron.* **35**, 1584–1589 (1999).
7. V. Wong and I. A. Walmsley, "Ultrashort-pulse characterization from dynamic spectrograms by iterative phase retrieval," *J. Opt. Soc. Am. B* **14**, 944–949 (1997).
8. K. W. DeLong, D. N. Fittinghoff, and R. Trebino, "Practical issues in ultrashort-pulse measurement using frequency-resolved optical gating," *IEEE J. Quantum Electron.* **32**, 1253–1264 (1996).
9. H. Fathallah, L. A. Rusch, and S. LaRochelle, "Passive optical fast frequency-hop cDMA communications system," *J. Lightwave Technol.* **17**, 397 (1999).
10. Coherent Lasers, <http://www.cohr.com>, Santa Clara, Calif.
11. Clark-MXR, Inc., <http://www.clark-mxr.com>, Dexter, Mich.
12. Brimrose Corporation of America, <http://www.brimrose.com>, Baltimore, Md.
13. LeCroy Corporation, <http://www.lecroy.com>, Chestnut Ridge, N.Y.
14. W. Yang, D. Keusters, D. Goswami, and W. S. Warren, "Rapid ultrafine-tunable optical delay line at the 1.55- μ m wavelength," *Opt. Lett.* **23**, 1843–1845 (1998).
15. K. D. Rector and M. D. Fayer, "Vibrational echoes: a new approach to condensed-matter vibrational spectroscopy," *Int. Rev. Phys. Chem.* **17**, 261 (1998).
16. N. F. Scherer, R. J. Carlson, A. Matro, M. Du, A. J. Ruggiero, V. Romerorochin, J. A. Cina, G. R. Fleming, and S. A. Rice, "Fluorescence-detected wave packet interferometry time-resolved molecular spectroscopy with sequences of femtosecond phase-locked pulses," *J. Chem. Phys.* **95**, 1487 (1991).